


Microstructural Characteristics and Wear Behavior of Sintered Ni-Modified Ti–xTiB₂ Composites

Oluwasegun Eso Falodun^{1,2}  · Samuel Ranti Oke^{2,3} · Peter Apata Olubambi² · Joseph Osekhoghene Dirisu¹ · Rasidi Sule⁴

Received: 20 January 2023 / Accepted: 8 April 2023 / Published online: 19 April 2023
© The Author(s) 2023

Abstract Titanium matrix composites were manufactured using pulsed plasma sintering with the addition of 5 wt.% Ni and TiB₂ (x = 5, 10, 15, 20 wt.%) particles at a sintering temperature of 1000 °C, a heating rate of 100 °C/min, and a holding time (300 s) at an applied pressure of 50 MPa. The study examines the densification, phase evolution, hardness, microstructure, and wear behavior of Ti–Ni alloys with different ceramic (TiB₂) contents. The results show that increasing TiB₂ content decreases relative density from 99 to 97% while increasing hardness from 229 to 586 HV_{0.1}. The addition of Ni particles resulted in laminar α-Ti with well-defined β-Ti grain boundaries. Furthermore, the microstructural studies have revealed a dual-phase beta and alpha Ti phase with uniformly dispersed TiB₂ content. As a result of the interactions between β-Ti and Ni during sintering, an intermetallic (Ti₂Ni) eutectoid phase was formed. The presence of Ni and TiB₂ particles reduces the average coefficient of friction, wear volume, and wear rate. Therefore, the reinforced titanium matrix composites wear track surfaces exhibited a combination of abrasive and adhesive wear modes.

Keywords Ti · Ni powder · Spark plasma sintering · Microstructure · Hardness · Wear behavior

Introduction

Titanium alloys have been employed in a broad range of modern and specialized applications due to their desirable properties such as low density, specific strength, biocompatibility, and exceptional oxidation resistance [1, 2]. Titanium-based alloys are viable and valuable in engineering applications, including aerospace, automobile, and biomedical. Despite the outstanding properties of titanium alloy, they have some disadvantages, such as poor hardness, poor wear, and oxidation resistance when compared to superalloys and stainless steels. These constraints make titanium alloy prone to ductile–brittle failure, a high friction coefficient, and limited high-temperature properties, which have restrained their usage in specific industrial applications [3–5]. The property enhancement of pure titanium has fostered the development of advanced titanium matrix composites using metallic and ceramic particles.

Increasing the mechanical properties of titanium alloys to overcome constraints can be accomplished through alloying and particle reinforcement. However, particulate strengthening has the potential to significantly improve the mechanical properties of metal matrix composites by allowing the second-phase particles to bear most of the load during deformation [6–10]. Titanium matrix reinforced with micro-sized ceramic particles has gained significant attention because of its resistance to heat, low density, and outstanding mechanical properties. Titanium diboride (TiB₂) is one of the most effective particle substances for strengthening and modifying the characteristics of titanium-based composites. Researchers have focused on ceramic materials (TiB₂) due to its

✉ Oluwasegun Eso Falodun
oefalodun@gmail.com; segzy201@gmail.com

¹ Department of Mechanical Engineering, Covenant University, Ota, Ogun State, Nigeria
² Centre for Nanoengineering and Advanced Materials, University of Johannesburg, Johannesburg, South Africa
³ Department of Metallurgical and Materials Engineering, Federal University of Technology, Akure, Ondo State, Nigeria
⁴ Department of Industrial Physics, Covenant University, Ota, Ogun State, Nigeria

outstanding features like mechanical strength, wear, impact resistance, and high-temperature materials. Its high melting temperature, hardness, resistance to chemical reactions, and mechanical properties have contributed to its wide range of applications [11–15]. Delbari et al. [16] synthesized Ti–TiB₂ composites using spark plasma sintering. They reported that adding TiB₂ particles decreased the elongation, modulus of rupture, and ultimate tensile strength of the sintered materials, while the hardness increased with TiB₂. However, ductility is a significant effect of pure titanium reinforced with TiB₂. Titanium matrix composites of more than 30% TiB₂ show almost zero ductility at room temperature. The ductility level decreased with an increased TiB₂ proportion.

However, incorporating ceramic particles into titanium matrix composites have some shortcomings [17, 18]. The inadequate bonding interaction between ceramic particles and titanium matrix due to insufficient wettability is a matter of concern, severely limiting the material's ability to be easily modified and functional. Another consideration is that when the added reinforcement content fraction exceeds a critical level, they prevent ceramic particulates from becoming well dispersed in the composite material during mechanical processing [19–21]. Because of these disadvantages, metal/metal matrix composites have emerged as a viable alternative due to their inherent good adhesion interaction synergy. Therefore, the ductility of titanium-based composites can be enhanced by adding different alloying elements, such as alpha, neutral, beta isomorph, and eutectoid stabilizers [22]. A small amount of nickel added to titanium increases its toughness, ductility, and sinterability. Nickel forms intermetallic compounds with titanium at high temperatures as a beta stabilizer [23]. These phases are ductile and have significant impact resistance and excellent damping abilities [24]. Nickel alloys create a solid solution with titanium, reinforcing and enhancing its mechanical properties for further usage because pure titanium is often unsuitable for several purposes [24]. The introduction of soft materials such as Ni might significantly reduce the enlargement of cracks in the course of sintering because of their superior oxidation resistance [25].

The processing method utilized in composite synthesis substantially impacts the materials structure and resulting mechanical properties. Titanium matrix composites with exceptional wear and mechanical properties have been manufactured utilizing powder metallurgy processing technologies, including microwave, hot isostatic pressing, and spark plasma sintering routes [26, 27]. This processing approach (SPS) has received much interest among the synthesis methods described above due to its distinctive properties as well as the prospect of producing near-net-shape composite materials. This work used spark plasma sintering to produce titanium matrix composites strengthened with Ni and TiB₂ particles. Spark plasma sintering is a

powder-forming technology that enables for lower sintering temperatures, faster heating, and cooling times [28]. This technology minimizes the possibility of unfavorable transformation between the reinforcement and the matrix structure [29]. The approach has shown to be viable for compacting powders to attain near theoretical density while requiring lower sintering time and temperature [30]. Spark plasma sintering effectively promotes atomic diffusion, preventing grain growth, and regulates the microstructures, sustaining grain size, and increasing the mechanical properties with high relative densities quickly [30, 31].

In this study, Ti alloy (grade 4) was reinforced with Ni and TiB₂ particles by applying the pulsed plasma sintering technique. The Ni particle was added to enhance sinterability and retain some elastic properties in the composites. As a result, the incorporation of Ni and TiB₂ ceramic additions on microstructural characteristics, densification, hardness, and wear behavior of spark plasma sintered Ti–Ni–TiB₂ composites was investigated.

Materials and Method

The raw materials used in this study are Ti alloy (grade 4), Ni, and TiB₂ powders. A planetary ball mill machine (PM 400 model) was used during the mixing procedure to achieve uniform dispersion of each element powder within the matrix and reinforcement. The Ti–Ni–TiB₂ composite mixture was prepared in an alumina container using the following parameters: rotational speed = 15.70 rad/s, mixing time = 8 h, ball-to-powder ratio = 10:1, alumina milling balls = 10 mm diameter, and holding time interval of 10 min to avoid heating the powders, cold welding the particles, and forming undesired phases within the powders during the mixing procedure. The powder mixture was placed in a graphite die and sintered with the help of pulsed plasma sintering equipment (HHPD-25 model, Germany) in a vacuum atmosphere. The following was the sintering conditions: sintering temperature of 1000 °C, heating rate of 100 °C/min, pressing force of 50 MPa, and 300 secs hold interval in a closed vessel. After sintering, the Ti–Ni matrix composite was blasted to eliminate the graphite sheet used to enclose the punches and die components. All samples were in the shape of 20 mm plates with a 5 mm height.

The Ti–Ni-based composites relative density was calculated using the Archimedes method and the ASTM B962-15 specification. The samples were immersed in deionized water and measured using an electronic measuring device. The hardness was performed on a cross-section area using a microhardness Vickers machine (FALCON 500 series) with a load of 200 gf and a dwell duration of 10 s. The phases of the sintered composites were studied using X-ray diffraction (Philip PW1710) to determine the presence of all

phases. However, Xpert Software assessed all phases present in the sintered composite. The titanium matrix composite was cut, grind, and polished before being etched with Kroll's reagent for microstructural analysis. The characterization was conducted using a field scanning electron microscope (JEOL JSM-7600 F model) coupled with an energy-dispersive spectrometer (accelerating voltage = 15 kV).

A tribometer pin-on-disk friction module approach was used to perform the wear test. A Stainless-steel ball of $\phi 6$ mm was used as a counterface material that slides against the sintered titanium matrix composite. A contact force of 1.0 kgf and a spindle speed of 31.42 rad/s were performed in ambient conditions. The wear tests of the composites were analyzed as a function of sliding time, and the coefficient of friction for each material was reported. The worn volumes and wear rates were determined. The following Eqs. (1) and (2) below were utilized:

$$V = \frac{\delta w}{\rho} \quad (1)$$

δw = change in weight (initial–final) test and ρ = density of the materials. Using Eq. (2), the wear rate (W) was calculated:

$$W = \frac{\delta w}{L \cdot \rho \cdot F} \quad (2)$$

Therefore, δw = (weight loss difference), ρ is the density, L represents the slide range, and F represents the pressing load.

Results and Discussion

Powder Processing and Characterization

Figure 1a–c depicts the powder microstructure of titanium, nickel, and ceramic (TiB_2) particles. Ti powder has a ball-shaped, non-porous structure, as shown in Fig. 1a. However, some other satellites cluster together and adhere to larger titanium powder particles. Figure 1c shows that the ceramic (TiB_2) powder consists of irregularly shaped particles, while Fig. 1d and e revealed that the Ni and TiB_2 particles were uniformly dispersed on the surfaces of the Ti powder, and there was good metallurgical interfacial bonding between the powder particles. However, we can see that a few agglomerating particles, possibly from cold welding, cause powder bonding at the interface during the mixing process. As a result, the quality of the powder blending method is used to determine the homogeneity of the dispersed particles [32]. The SEM–EDX analysis confirms the elements after the dispersion of Ni– TiB_2 particles into the Ti matrix, as shown in Fig. 1f.

The X-ray diffraction analysis was used to determine whether a chemical reaction occurred during powder mixing. The phases present in the admixed powders are presented in Fig. 2. The diffraction pattern shows that the sintered titanium matrix composites consist of peaks corresponding to α -Ti, Ni, and TiB_2 , with reflections matching TiB. The evolution of the TiB phase explains that an in-situ reaction exists between Ti and TiB_2 during powder mixing. The TiB and TiB_2 peaks were present in the composites reinforced with 5–15 wt.% TiB_2 ; this suggests that there is not sufficient SPS processing time to accelerate a complete reaction between Ti and TiB_2 . However, the peaks related to the TiB_2 phase disappeared in the XRD pattern of the composite reinforced with 20 wt.% TiB_2 ; this indicates a total chemical reaction between the TiB_2 and Ti matrix. The in-situ transformation of TiB_2 to TiB phase in the composite is described in Eq. (3):



Figure 3a–c depicts the influence of TiB_2 ceramic particles on the sintering pattern, displacement, and shrinkage rate of sintered composite materials as against time. The sintering temperature was steady at 250 °C for about 7 min, then elevated to 1000 °C, kept for 300 s, and cooled to room temperature, according to the sintering profile (Fig. 3a). Figure 3b shows that when the temperature rises, the displacement increases due to the rearrangement of the powders and the influence of pressure applied, which causes a discharge of trapped air and gas within the compact. Due to these combined actions, the sintering process is accompanied by neck growth [33]. As a result, an increase in displacement behavior indicates that the powders physical state and structure have changed. The shrinkage rate (Fig. 3c) is a method used to investigate the deformation behavior of the composite during spark plasma sintering. In the graph, there are just two shrinkage peaks. The first shrinkage step is attributed to the Joule heating effect, which was complemented by enormous plastic deformation of the particles at the contact point. This stage has been observed to cause powder surface activation, partially melting at powder contact points, developing a neck at contact points, atomic diffusion, and plastic flow [34]. Densification is accelerated at this point and continues progressing via plastic deformation under pressure. In the second stage, there was a significant reduction in shrinkage, which could be due to a drop in temperature produced by cooling the furnace chamber to ambient temperature. Densification is thus completed by mass transportation [35].

Relative Density and Microhardness Test

Figure 4 depicts the significance of Ni and ceramic particles (TiB_2) on relative density and microhardness values.

Fig. 1 SEM image of the powders particles; **a** Ti, **b** Ni, **c** TiB_2 , **d–f** mixed particles containing 10 and 20 wt.% TiB_2 with EDX analysis

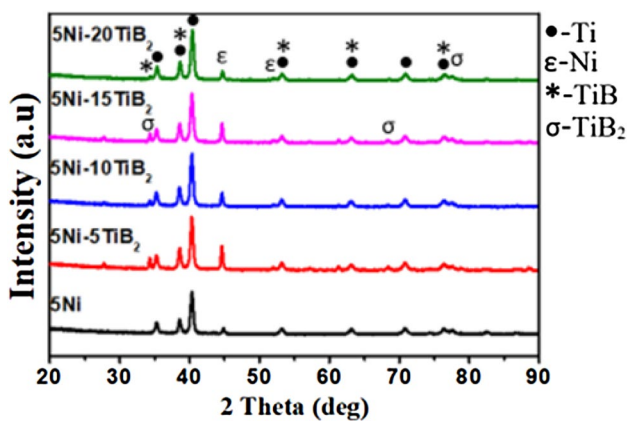
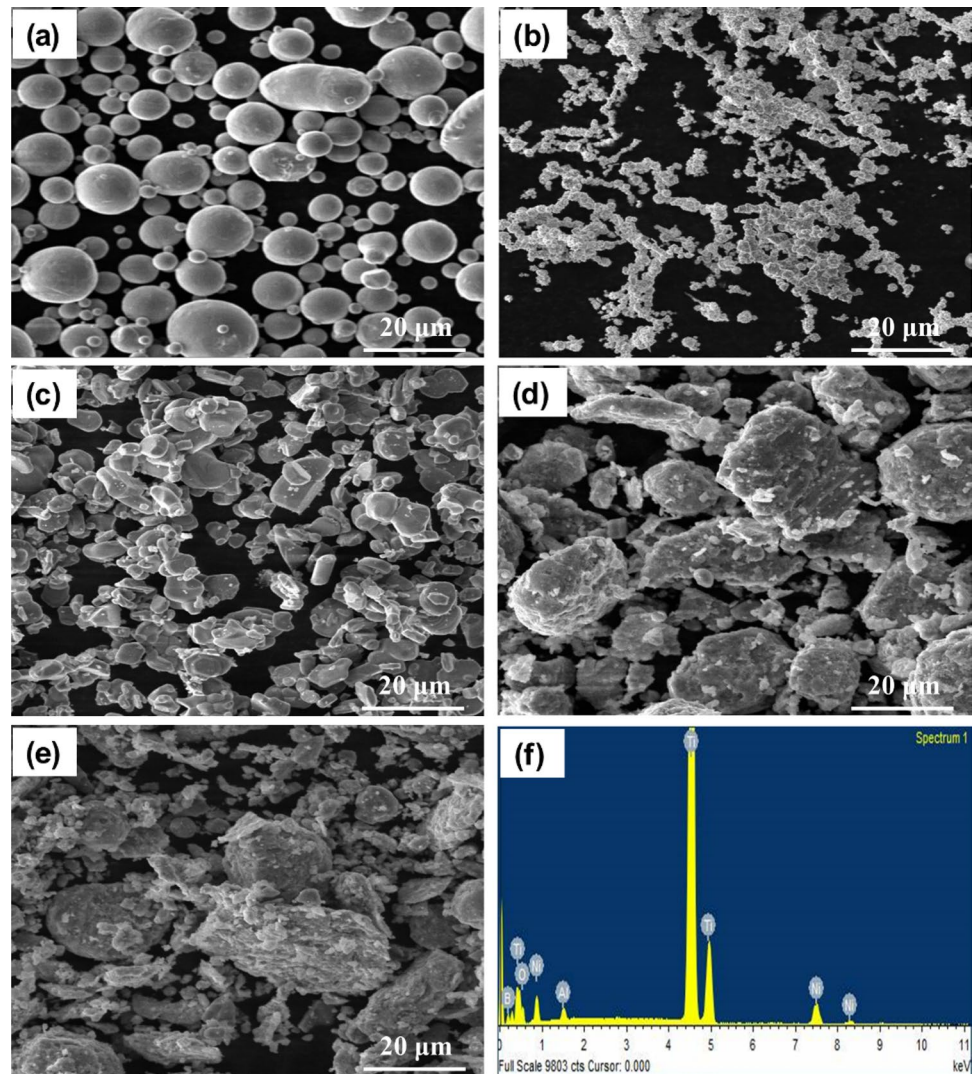


Fig. 2 X-ray diffraction analysis of admixed particles

It is observed that incorporating ceramic reinforcement into the Ti–Ni matrix decreases their relative density with an increase in TiB_2 reinforcement from 5 to 20 wt.%. The

reduction in relative density indicates that the composite material may contain some porosity [36]. As the ceramic particle (TiB_2) content increases, the microhardness of the Ti–Ni composite increases, as shown in Fig. 4b. The increase is linked to the high hardness characteristics of ceramic additives. Moreover, the ceramic particle (TiB_2) restricts dislocation motion and is an excellent barrier against permanent material distortion [37]. The uniform dispersion of the reinforcing phases and increase in the number of grain boundaries prevent dislocation slip, which is responsible for increase in the hardness of the titanium matrix composite. Furthermore, the addition of Ni particles also improved the plasticity.

Microstructure Characterization

Figure 5 depicts SEM micrographs of Ti–Ni composites with various TiB_2 contents. Figure 5a shows that the microstructure predominantly composed of α -Ti phases with a lamellar

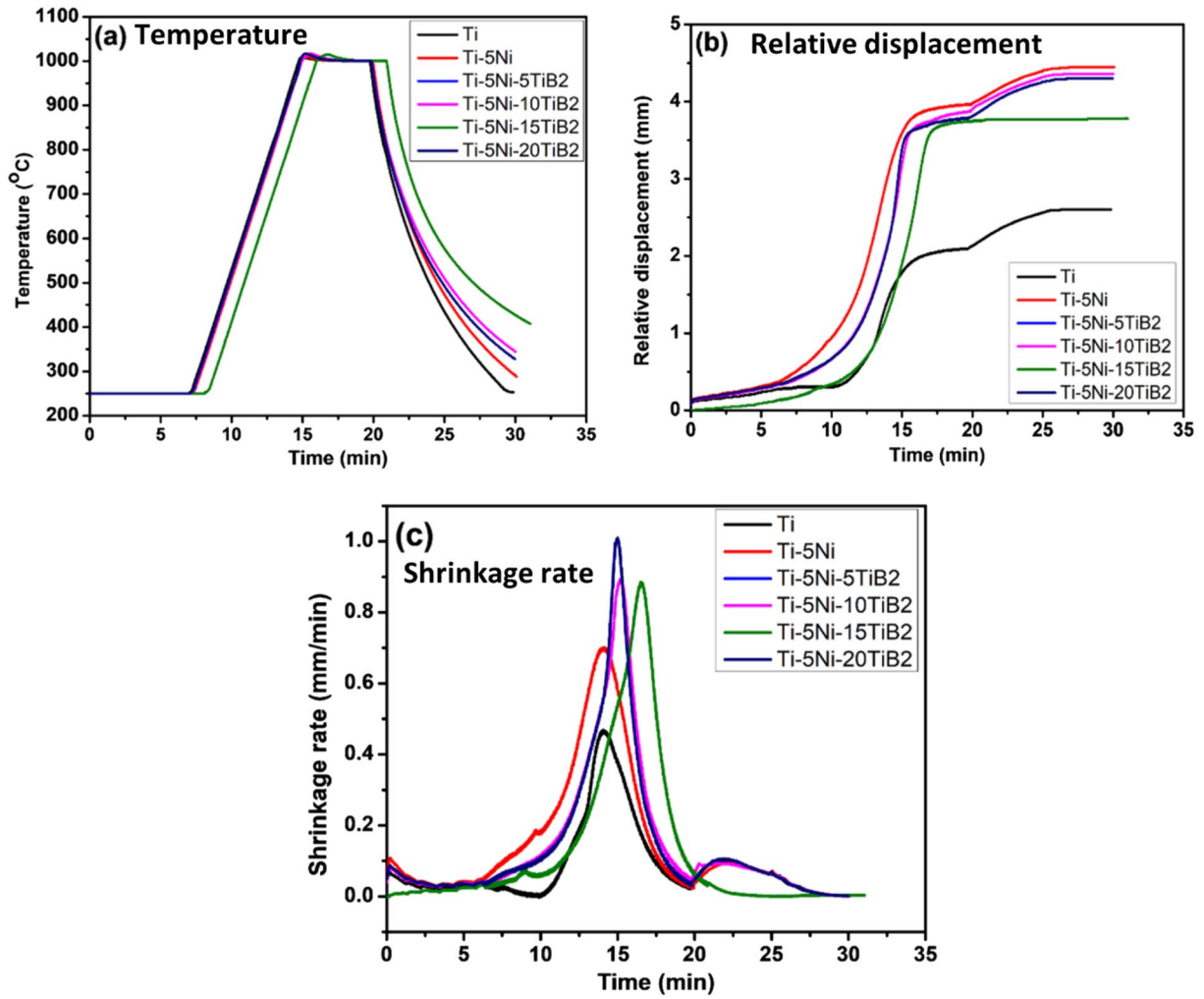


Fig. 3 Spark plasma sintering conditions against time

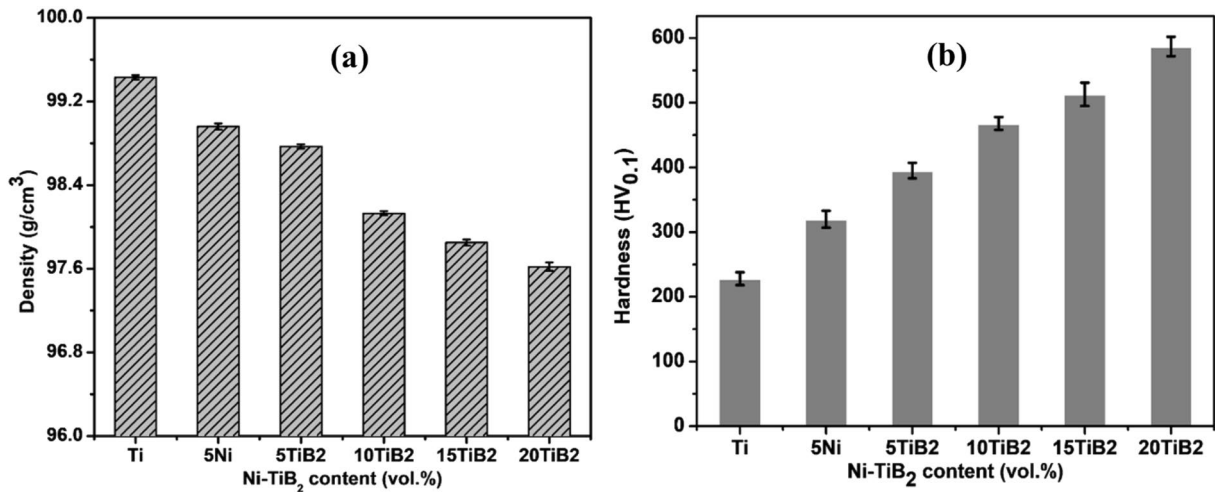
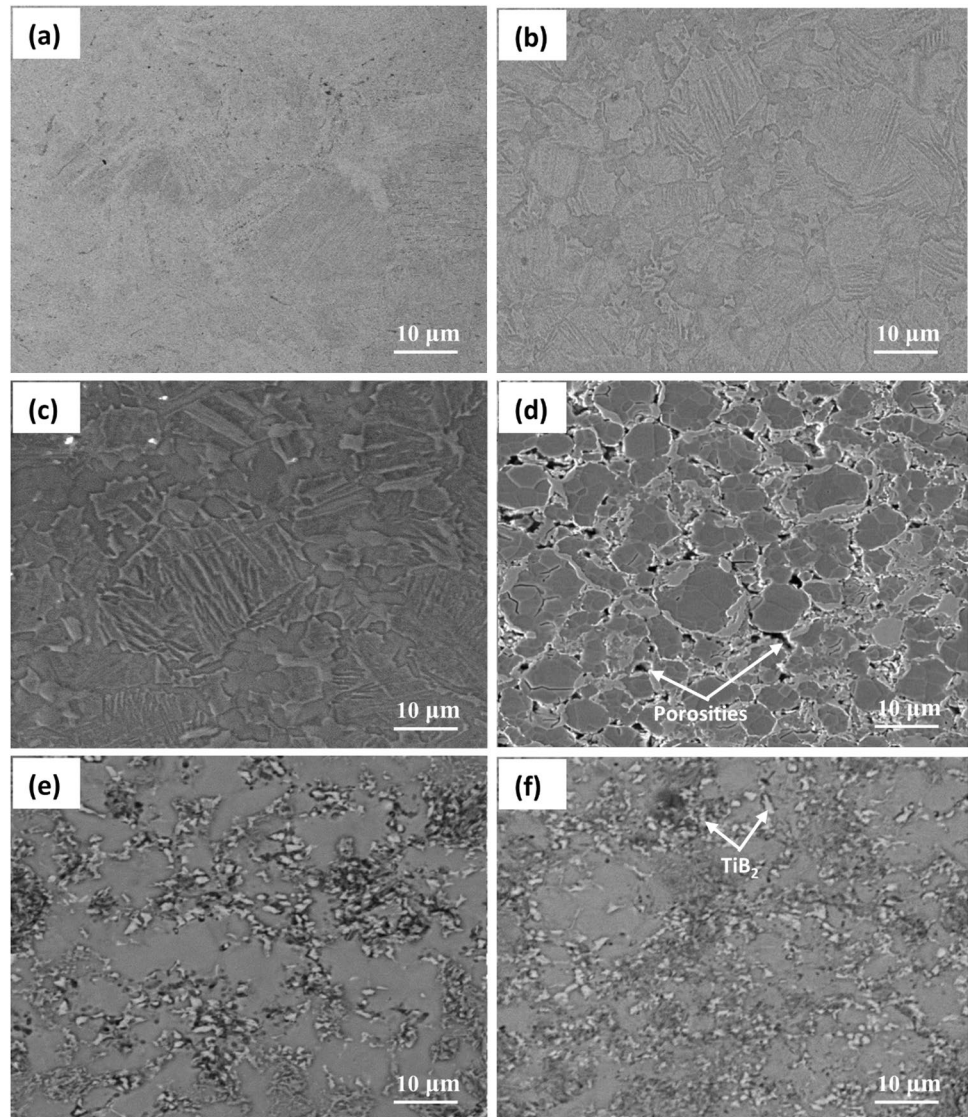


Fig. 4 a Relative density and b microhardness values

structure. However, the addition of Ni–TiB₂ particles in Fig. 5b–e causes a formation of α phase with well-defined β grain boundaries in the composites. This transformation causes intermetallic phases, attributed to interfacial reaction between the reinforcement and matrix powder during the sintering [8]. The sintering of Ti alloy with Ni addition at 1000 °C influences the β transus temperature to form a stable β -Ti phase due to Ni being a β stabilizing element. Due to fast cooling associated with the sintering process, the transformation of β -Ti to α -Ti is incomplete, resulting in a mixture of laminar α with β grain boundaries. As a result of the interactions between β -Ti and Ni during sintering, an intermetallic (Ti₂Ni) eutectoid phase was formed. Figure 5c–f presents the microstructure of the Ti–Ni alloy reinforced with 5–20 wt.% TiB₂, respectively. SEM examination of the composite containing 5 wt.% TiB₂ (Fig. 5c) shows laminar α structure but with an increased grain size. When Ni–TiB₂

was added to Ti, the second phases were located near the Ti boundaries, which also inhibit the grain growth of Ti. Furthermore, the addition of ceramic particles (10 wt.% TiB₂) to the Ti matrix created a significant interface and formation of some void sites due to poor interfacial bonding between the reinforcement and matrix phases [38] as shown in Fig. 5d. It is important to emphasize that Ni atoms have a higher diffusion possibility than Ti atoms [20], and the created vacancies tend to aggregate close to the interface or dislocation. Figure 5e and f shows that the microstructure gradually transforms into an equiaxed structure as Ni–TiB₂ diffuses into the Ti matrix, and the vacancy concentration at the interface decreases and voids disappear completely. The observation indicates that the strengthening phase consists of microsized particles. However, the TiB₂ particles and a dual-phase matrix structure comprising beta and alpha titanium were evident in the Ti–Ni–TiB₂ composites.

Fig. 5 Microstructure micrographs of titanium–nickel alloy reinforced with ceramic particle (wt.%): **a** titanium alloy, **b** 5 Ni, **c** 5 TiB₂, **d** 10 TiB₂, **e** 15 TiB₂, and **f** 20 TiB₂



Phase Analysis

Figure 6 shows the XRD patterns of commercially pure titanium alloy with Ni and varying volume fractions of TiB_2 at a sintering temperature of 1000°C and their corresponding phases. The predominant phase observed in the pure Ti without Ni and TiB_2 is that of α -Ti; this is in line with the result of the EDS analysis, which revealed α -Ti as the only identifiable peak. The addition of Ni initiated and propagated the transformation of α -Ti to β -Ti observed at diffraction angles of 54° and 72° . The inclusion of the reinforcement phase into titanium alloy reduces peak intensities, with a slight change in the peaks, which could be due to the high tensile stress of the α phase [39]. Furthermore, the diffraction peaks validated the formation of dominant phases (α and β) [40]. It is evident that the increase in diffraction peak was attributed to the addition of ceramic particles. Also, the reduction in diffraction peaks could be traced directly to the X-ray absorption characteristic [40]. The new intermetallic peaks of TiNi_2 and Ti_2Ni evolved in the titanium matrix composites. However, the reduction in diffraction peaks is related to the TiB_2 phase. The absence of Ni spectra in the diffraction patterns indicated that the nickel alloy had interacted with titanium alloy to form an intermetallic phase [23].

Wear Behavior and Worn Surfaces Analysis

Figure 7a and b, respectively, depicts the titanium-based composites at a contact force of 1.0 kgf. The samples displayed similar behavior in the coefficient of friction characterized by an initial increase before stabilizing the coefficient of friction. This behavior is influenced by irregularity

and the frictional force that occurs during the specimen and the counter surface. The friction coefficient varies due to repeated coalescence and breakage of the thickness removal in the asperity zones of the specimen. The incorporation of 5 wt.% Ni increases the friction coefficient compared to the matrix specimen, whereas further addition of ceramic particles (5–15 wt.% TiB_2) decreases the coefficient of friction. The decrease in coefficient of friction caused by the addition of Ni and TiB_2 is due to the adhesive action of TiB_2 on the surface of the specimen, which forms a layer on the contacting surfaces, which further significantly lowers slides at the specimen and counter surfaces. However, it was observed that an increase in the coefficient of friction for 20 wt.% TiB_2 shows that bonding increased in the specimen and the counter surface [41].

Figure 8a and b presents the Ti–Ni matrix composites wear volume and wear rate subjected to a 1.0 kgf load. The wear volume and rate generally decreased with the addition of Ni particles. Further reduction in the volume and speed is evident with the TiB_2 particles in the titanium matrix. The significant reduction in wear volumes and rates demonstrates that TiB_2 particle addition improves composite wear performance under dry conditions when compared to titanium alloy. The associated reduction in wear volume and rate with Ni and TiB_2 additions might be linked to the high hardness of the TiB_2 phase. According to the titanium matrix composite microstructure (Fig. 5), the intermetallic formed during sintering may also influence the decrease. Another factor contributing to the decreased wear volumes and rates with higher content of TiB_2 particles is the reduction in the extent of plastic deformation during dry wear. A similar observation has been reported in reducing plastic deformation with microsized ceramic particles.

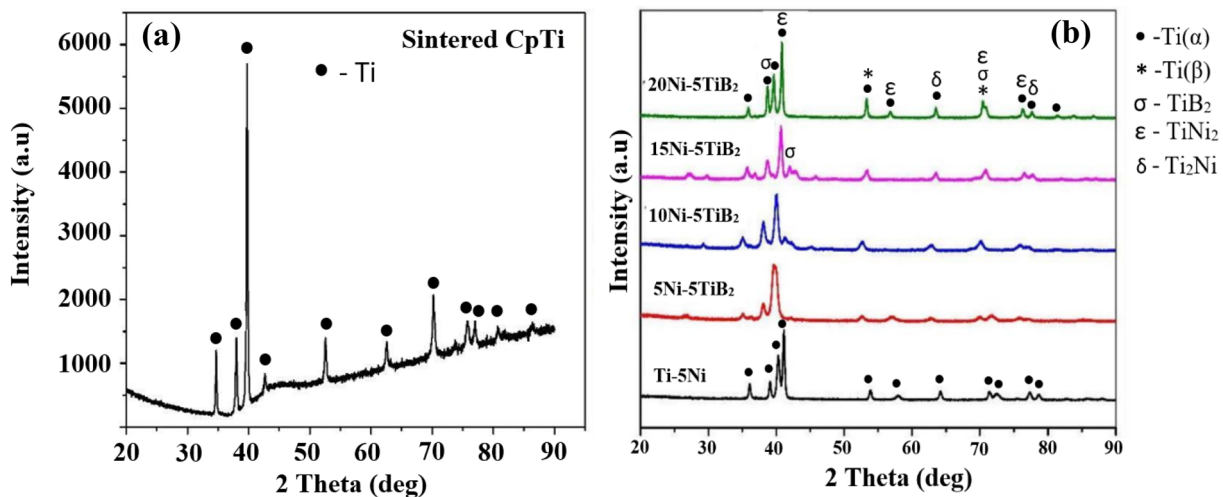


Fig. 6 Phase identification using X-ray diffraction patterns: **a** Ti and **b** Ti–Ni matrix composite (TiB_2 inclusion)

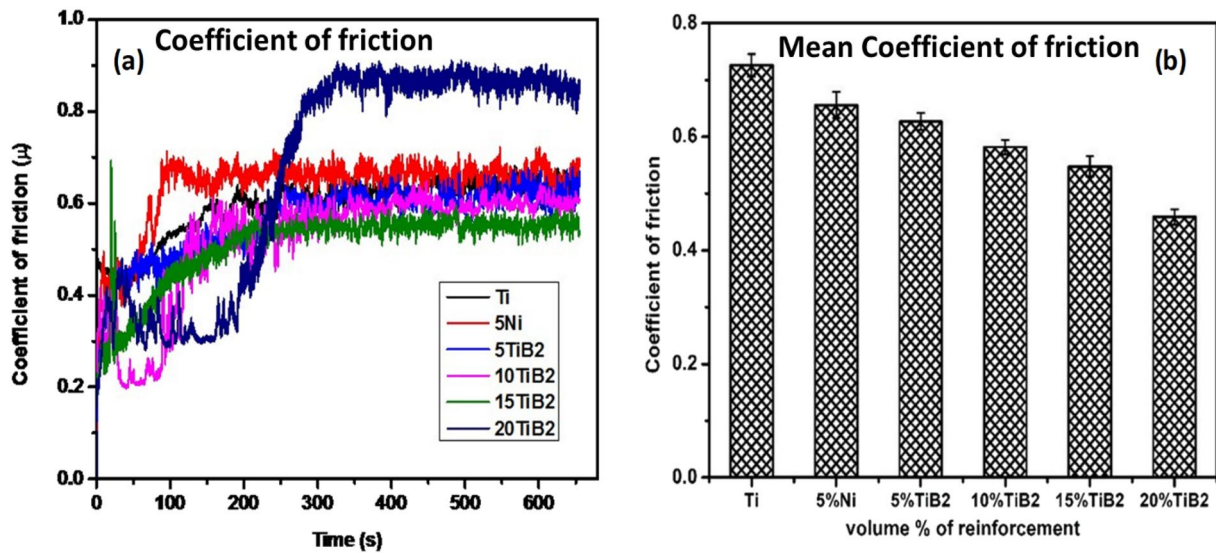


Fig. 7 Coefficient of friction and mean (COF) graphs

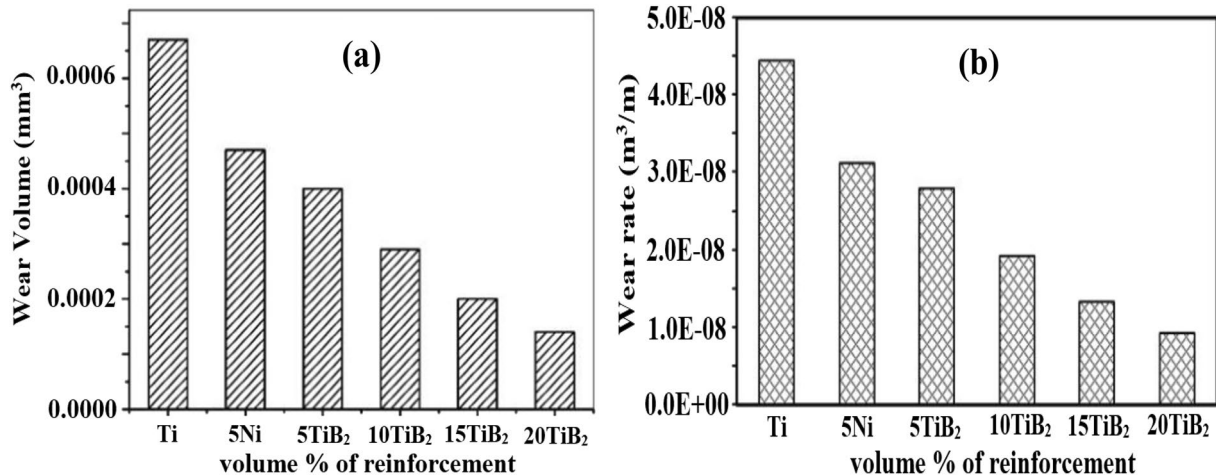


Fig. 8 Variation of wear reinforcing phase a wear volume and c wear rate

Figure 9 depicts the representative micrographs showing wear tracks of the pure titanium, 5 and 20 wt.% TiB₂ composite (a, b, and c), and their corresponding wear debris (a1, b1, and c1). Shallow, continuous, smooth, and parallel grooves lengthways of the sliding direction were evident in the pure titanium without any reinforcement (Fig. 9a). The dominant wear mechanism in the sintered titanium is abrasive; this might result from the low hardness of titanium and the absence of TiB₂ to resist plastic deformation on the surface [42, 43]. The micrographs of the degraded surface

of the 5 and 20 wt.% TiB₂ reinforced composite (Fig. 9b, c) revealed worn surfaces consisting of rough but continuous grooves with adhering tribolayers on the surface of the titanium matrix composites. The tribolayers help reduce heat generated on the composite sample surface during wear and direct contact between the sample and the counterface ball. This reduces the coefficient of friction and enhances resistance to plastic deformation of the surface of the composite. For the TiB₂ reinforced composites, the wear track surfaces have both abrasive and adhesive wear modes.

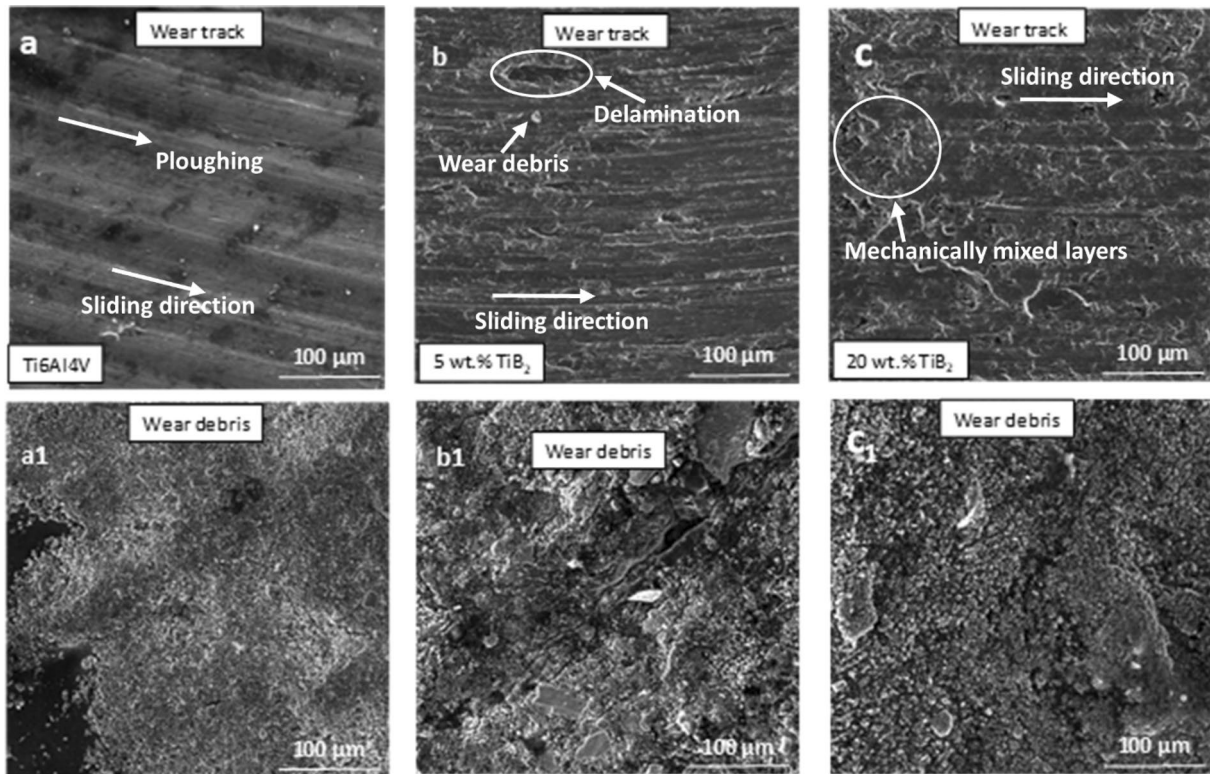


Fig. 9 Scanning electron morphologies of sintered worn tracks (a, b, and c) and wear debris (a1, b1, and c1)

Conclusion

1. The dispersion and strengthening of Ni–TiB₂ particles into the Ti matrix produced homogeneous distribution and good metallurgical interfacial bonding between the powder particles.
2. Ti alloy microstructure predominantly composed of α -Ti phases with a lamellar structure. However, the addition of Ni–TiB₂ particles to Ti causes a formation of α phase with well-defined grain boundaries (second phase) located near the grain boundaries. As a result of the transformation, intermetallic phases form due to the interfacial reaction between the reinforcement and matrix powder during sintering.
3. The microhardness increases with the ceramic particle increase. The microhardness increases with the varying content (wt.%) of ceramic particles. Although a decrease in the composite relative density with increasing reinforcement concentration suggests that the composite material may contain porosities.
4. The inclusion of Ni–TiB₂ particles in the Ti matrix reduces the coefficient of friction, wear volume, and the wear rate. The addition of TiB₂ particles improves wear performance in dry conditions. The reinforced titanium

matrix composites exhibited a combination of abrasive and adhesive wear modes.

Acknowledgements The authors would like to appreciate Covenant University, Ota, Nigeria and University of Johannesburg, South Africa for their support.

Funding Open access funding provided by University of Johannesburg. The authors have not disclosed any funding.

Declarations

Conflict of interest The authors declare no competing interests.

Open Access This article is licensed under a Creative Commons Attribution 4.0 International License, which permits use, sharing, adaptation, distribution and reproduction in any medium or format, as long as you give appropriate credit to the original author(s) and the source, provide a link to the Creative Commons licence, and indicate if changes were made. The images or other third party material in this article are included in the article's Creative Commons licence, unless indicated otherwise in a credit line to the material. If material is not included in the article's Creative Commons licence and your intended use is not permitted by statutory regulation or exceeds the permitted use, you will need to obtain permission directly from the copyright holder. To view a copy of this licence, visit <http://creativecommons.org/licenses/by/4.0/>.

References

1. I. Gurrappa, *Mater. Charact.* **51**, 131 (2003)
2. O.E. Falodun, B.A. Obadele, S.R. Oke, O.O. Ige, P.A. Olubambi, *Part. Sci. Technol.* **38**, 156 (2020)
3. A. Muthuchamy, M. Rajadurai, A.R. Annamalai, D.K. Agrawal, *Trans. Indian Inst. Met.* **72**, 2127 (2019)
4. M. Long, H.J. Rack, *Biomaterials* **19**, 1621 (1998)
5. D. Banerjee, J.C. Williams, *Acta Mater.* **61**, 844 (2013)
6. V.M. Tabie, J.K. Quaisie, J. Li, P. Yamba, X. Xu, *Eur. Phys. J. Appl. Phys.* **98**, 3 (2023)
7. A.L. Rominiyi, P.M. Mashinini, *Int. J. Adv. Manuf. Technol.* **124**, 709 (2023)
8. Y. Wang, M. Zhu, L. Dong, G. Sun, W. Zhang, H. Xue, Y. Fu, A. Elmarakbi, Y. Zhang, *J. Alloys Compd.* **947**, 169557 (2023)
9. J.O. Abe, O.M. Popoola, A.P.I. Popoola, *JOM* **75**, 791 (2023)
10. D.C. Zhang, Y.F. Mao, Y.L. Li, J.J. Li, M. Yuan, J.G. Lin, *Mater. Sci. Eng. A* **559**, 706 (2013)
11. O.E. Falodun, S.R. Oke, S.O. Akinwamide, O.O. Ajibola, A.O. Adebayo, S.G. Borisade, A.A. Adediran, P.A. Olubambi, *J. Mater. Eng. Perform.* (2022). <https://doi.org/10.1007/s11665-022-07504-x>
12. C. Subramanian, T.S.R.C. Murthy, A.K. Suri, *Int. J. Refract. Met. Hard Mater.* **25**, 345 (2007)
13. E. Bilgi, H.E. Camurlu, B. Akgün, Y. Topkaya, N. Sevinç, *Mater. Res. Bull.* **43**, 873 (2008)
14. A. Jain, R. Pankajavalli, S. Anthonysamy, K. Ananthasivan, R. Babu, V. Ganesan, G.S. Gupta, *J. Alloys Compd.* **491**, 747 (2010)
15. O.O. Ayodele, B.J. Babalola, P.A. Olubambi, *J. Mater. Res. Technol.* **17**, 2807 (2022)
16. S.A. Delbari, A.S. Namini, M.S. Asl, *Mater. Today Commun.* **20**, 100576 (2019)
17. Y. Bao, L. Huang, S. Jiang, R. Zhang, Q. An, C. Zhang, L. Geng, X. Ma, *J. Mater. Sci. Technol.* **83**, 145 (2021)
18. A.S. Namini, S.A.A. Dilawary, A. Motallebzadeh, M.S. Asl, *Compos. Part B Eng.* **172**, 271 (2019)
19. H. Singh, M. Hayat, Z. He, V.K. Peterson, R. Das, P. Cao, *Compos. Part A Appl. Sci. Manuf.* **124**, 105501 (2019)
20. Y. Xiong, F. Zhang, Y. Huang, C. Shang, Q. Wan, *Mater. Sci. Eng. A* **859**, 144235 (2022)
21. D. Wang, D. Sun, X. Han, Q. Wang, *Mater. Sci. Eng. A* **742**, 231 (2019)
22. W.D. Callister, D.G. Rethwisch, *Materials Science and Engineering: an Introduction* (Wiley, New York, 2018)
23. A.L. Rominiyi, M.B. Shongwe, E.N. Ogunmuyiwa, B.J. Babalola, P.F. Lepele, P.A. Olubambi, *Mater. Chem. Phys.* **240**, 122130 (2020)
24. C. Machio, M.N. Mathabathe, A.S. Bolokang, *J. Alloys Compd.* **848**, 156494 (2020)
25. B.V.M. Kumar, J.R. Kumar, B. Basu, *Int. J. Refract. Met. Hard Mater.* **25**, 392 (2007)
26. A.M. Okoro, S.S. Lephuthing, S.R. Oke, O.E. Falodun, M.A. Awotunde, P.A. Olubambi, *JOM* **71**, 567 (2019)
27. O.E. Falodun, B.A. Obadele, S.R. Oke, A.M. Okoro, P.A. Olubambi, *Int. J. Adv. Manuf. Technol.* **102**, 322 (2019)
28. V. Mamedov, *Powder Metall.* **45**, 322 (2002)
29. M. Farvizi, M. Ghanbariha, A. Faraji, *Met. Mater. Int.* **27**, 5407 (2021)
30. H. Feng, Y. Zhou, D. Jia, Q. Meng, *Mater. Sci. Eng. A* **390**, 344 (2005)
31. O.E. Falodun, B.A. Obadele, S.R. Oke, M.E. Maja, P.A. Olubambi, *J. Alloys Compd.* **736**, 202 (2018)
32. A. Couret, G. Molénat, J. Galy, M. Thomas, *Intermetallics* **16**, 1134 (2008)
33. Z.H. Zhang, X.B. Shen, F.C. Wang, S.K. Lee, L. Wang, *Mater. Sci. Eng. A* **527**, 5947 (2010)
34. S.R. Oke, O.O. Ige, O.E. Falodun, A.M. Okoro, M.R. Mphahlele, P.A. Olubambi, *Int. J. Adv. Manuf. Technol.* **102**, 3271 (2019)
35. S. Diouf, A. Molinari, *Powder Technol.* **221**, 220 (2012)
36. M. Ipekoglu, A. Nekouyan, O. Albayrak, S. Altintas, *J. Mater. Res.* **32**, 599 (2017)
37. O. E. Falodun, B. A. Obadele, S. R. Oke, M. E. Maja, P. A. Olubambi, in *IOP Conference Series: Materials Science and Engineering* (2017)
38. O.E. Falodun, S.R. Oke, B.A. Obadele, A.M. Okoro, P.A. Olubambi, *Met. Mater. Int.* **27**, 1769 (2021)
39. A. Amanov, B. Urmanov, T. Amanov, Y.S. Pyun, *Mater. Lett.* **196**, 198 (2017)
40. O.E. Falodun, B.A. Obadele, S.R. Oke, P.A. Olubambi, J. Westraadt, *Mater. Res. Bull.* **117**, 90 (2019)
41. E. Nsiah-Baafi, A. Andrews, S. Diouf, P.A. Olubambi, *Open Ceram.* **10**, 100260 (2022)
42. O.E. Falodun, B.A. Obadele, S.R. Oke, O.O. Ige, P.A. Olubambi, M.L. Lethabane, S.W. Bhero, *Trans. Nonferrous Met. Soc. China* **28**, 47 (2018). (English Ed.)
43. O.O. Ayodele, M. Awotunde, M.B. Shongwe, A.O. Adegbenjo, B.J. Babalola, B.A. Obadele, P.A. Olubambi, *Key Eng. Mater.* **821**, 321–326 (2019)

Publisher's Note Springer Nature remains neutral with regard to jurisdictional claims in published maps and institutional affiliations.